Bulletin of the Seismological Society of America, Vol. 107, No. 1, pp. –, February 2017, doi: 10.1785/0120160156

In Situ Stress and Active Faulting in Oklahoma

by Richard C. Alt II and Mark D. Zoback

Abstract Appreciable injection-induced seismicity has been occurring in north-central Oklahoma since 2009. To better understand these earthquakes, we have compiled new information on the state of stress in the state to compare it with both mapped faults and faults inferred from earthquake epicenters and focal plane mechanisms. Seventy-five new *in situ* stress orientations are available from wellbores throughout the state. In the north-central part of the state where the induced seismicity is occurring, stress orientation and relative magnitude from focal mechanism inversions show excellent agreement with the wellbore stress orientations. All of the data show remarkably uniform stress directions. The azimuth of S_{Hmax}, the maximum horizontal stress, is about N85°(±5°)E. Strike-slip faulting is occurring in central Oklahoma, with strike-slip/normal and normal faulting observed in northern Oklahoma and southern Kansas. As very few of the thousands of $\mathbf{M} \geq 2.5$ earthquakes that have recently occurred are located on, or near, already mapped faults, we utilize the stress information to interpret the likely fault planes associated with over 300 well-constrained focal plane mechanisms. In the vicinity of the January 2016 sequence of magnitude 4 and 5 earthquakes in the Fairview, Oklahoma, region, we illustrate how knowledge of the stress field can be used to identify the faults responsible for the seismicity and better evaluate the potential hazard associated with possible future earthquakes in the area. The September 2016 M_{w} 5.8 Pawnee event occurred on an unmapped N70°W trending strike-slip fault expected to be active in the local stress field.

Introduction

Over the past six years, earthquake activity in north-central Oklahoma has reached unprecedented levels for intraplate regions in North America (Fig. 1). On average, there was one magnitude 4 or larger earthquake each week in late 2015/early 2016, compared with a background rate of one per decade prior to 2009. Various studies have established links between oil and gas activities and these earthquakes (Keranen *et al.*, 2013, 2014), principally through the injection of enormous quantities of saltwater coproduced with oil (Walsh and Zoback, 2015a). Nearly all of the faults responsible for these earthquakes are poorly understood, making it difficult to assess seismic hazard.

To better understand the nature of faulting in the area of recent seismicity, we first present a detailed map of the tectonic stress field in Oklahoma based on newly available wellbore stress measurements. We then utilize this information in the context of Coulomb faulting theory to assess which focal plane, in over 300 well-constrained focal plane mechanisms, corresponds to the likely fault plane.

The new Oklahoma stress map shown in Figure 1 is principally based on observations of drilling-induced tensile fractures in electrical image logs in near-vertical oil and gas wells (see Data and Resources). At 63 sites, maximum horizontal stress (S_{Hmax}) orientations were determined from multiple observations of the azimuth of drilling-induced tensile fractures. In 12 wells, the fast azimuth of shear-velocity anisotropy in dipole sonic logs was used to determine stress orientation and yield similar results when both types of data are available in the same area (see Data and Resources). To evaluate the relative quality of the wellbore failure observations (and utilize the shear-velocity anisotropy in the analysis), we utilize (and extend) the Zoback and Zoback (1991) quality ranking system used by Zoback (1992a) for the World Stress Map project (see Table A1).

Figure 1 shows the 75 new stress orientations as well as 11 A and B quality data points available in the World Stress Map database (Heidbach *et al.*, 2010). All of the stress indicators are listed in Table A2. Because the data in the World Stress Map database come from stress-induced wellbore breakouts analyzed on paper copies of old 4-arm caliper logs, it is of lower quality than the new data reported here. Zoback (2007) reviews the wellbore stress orientation methodologies utilized in this study and World Stress Map compilation.

It is clear in Figure 1 that throughout much of the state (and especially in the region of recent seismicity), there is a consistent N80°–90°E orientation of the maximum horizontal principal stress S_{Hmax}. This uniform stress field appears to extend west into the Texas panhandle and is seen in

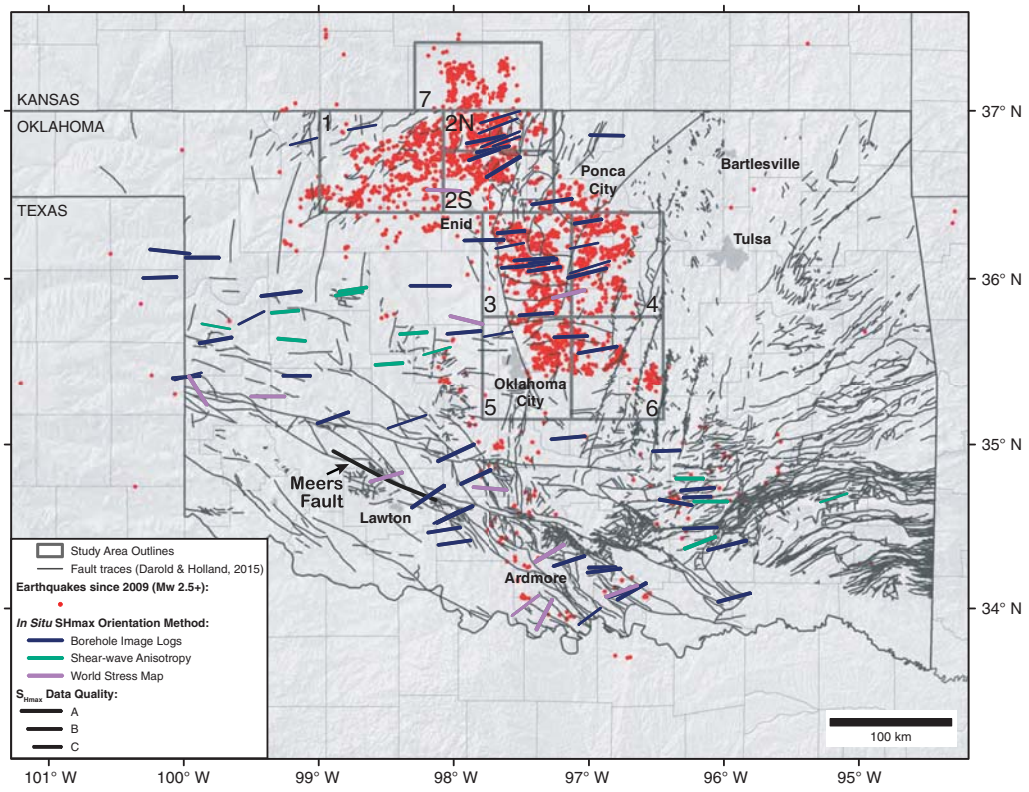

Figure 1. Oklahoma stress map. The symbols showing the orientation of S_{Hmax}, utilizing different sources of data (and data quality) as described in the legend. Earthquake epicenters for recent earthquakes (red dots) of **M** 2.5 and greater since 2009 (U.S. Geological Survey, 2016) and faults throughout the state compiled by the Oklahoma Geological Survey (Darold and Holland, 2015). The seven study areas shown are discussed in the text.

southeastern Oklahoma, northeast of Ardmore (Lund Snee and Zoback, 2016). In southern Oklahoma, we observe a deviation from this uniform field, with a counter-clockwise rotation of the S_{Hmax} azimuth toward the north, culminating in an approximately N50°E orientation near the Texas border south of Ardmore. There is a similar counter-clockwise stress rotation near Lawton. The Meers fault, which broke in a prehistoric **M** ~ 7 earthquake (Crone and Luza, 1990), is located in this area (Fig. 1). A 3-m fault scarp dated to 1100–1400 yrs using ^{14}C ages of disturbed (and undisturbed) deposits was likely formed in a single-slip event. The Meers fault is an oblique reverse fault, part of the frontal thrust system of the Amarillo–Wichita Uplift. The earthquake on the Meers fault is comparable in moment magnitude to the largest earthquakes of the 1811–1812 New Madrid sequence (Luza *et al.*, 1987; Luza, 1989; Crone and Luza, 1990). As there is evidence of recurring Pleistocene earthquakes on the fault, albeit with less precise dates, the Meers fault presents a substantial seismic hazard. Other active reverse faults have been inferred along the Wichita front in southwestern Oklahoma, but few earthquakes have occurred in the area.

Mapped Faults in Oklahoma

The faults shown in Figure 1 are a compilation by the Oklahoma Geological Survey (OGS; Darold and Holland, 2015). The map is based on faults described in published papers and those provided by the oil and gas industry on the basis of seismic and well data in sedimentary basins. Obviously, basement faults could be missed frequently if they do not offset overlaying sedimentary formations enough to be seen in seismic-reflection data. As seen in Figure 2, the majority of the earthquakes in north-central Oklahoma are not associated with mapped faults, even accounting for the 3–5 km uncertainty in epicenter locations (McNamara *et al.*, 2015). It is equally important to recognize that many mapped faults in the state reflect long-past tectonic events and are currently not active, although some may be reactivated in the current stress field. Oklahoma has generally been a tectonically quiescent region in Mesozoic and Cenozoic time, with little deposition since the Permian (e.g., Carter *et al.*, 1998). Furthermore, Quaternary sediments are subaerial, which, combined with slow slip rates, obscure even steeply dipping fault planes from view at the surface (e.g., Johnson, 1989; Carter *et al.*, 1998). Subsurface data are therefore essential to assemble a substantially accurate fault map. The major exception to this rule is along the Wichita, Arbuckle, and Ouachita Mountains in the far south of the state, where surface exposure of basement rocks allows for more faults to be identified. Although Oklahoma has been integrated into the intraplate United States midcontinent since the Paleozoic, a subset of faults that represent the imprint

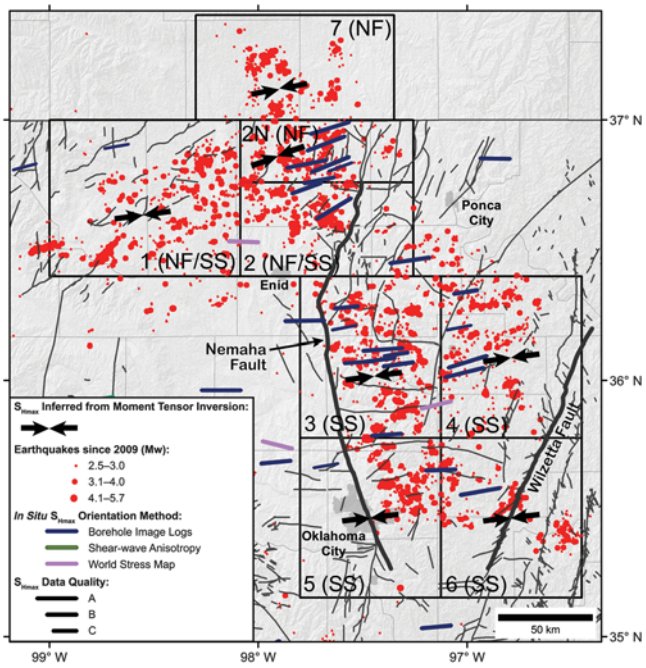

Figure 2. The stress map is enlarged on the seven study areas with stress orientation and style of faulting for each stress inversion plotted along with those borehole stress observations and earthquakes that fall here or within the region. Note that most of the earthquakes are not associated with the already mapped faults.

of past tectonic regimes will be well oriented to slip with minimal pore-pressure perturbation in the *in situ* stress state, thus accounting for the natural seismicity that occurs in the area.

In addition to the Meers fault, other prominent faults on this map include the Wilzetta fault (see also Fig. 2), a long north-northeast-trending strike-slip fault located about 100 km east of Oklahoma City. The earthquake sequence in November 2011 that included an M_w 5.6 event occurred on one of the splays near the town of Prague (e.g., Keranen *et al.*, 2013; McNamara *et al.*, 2015). Prior to this earthquake sequence, this particular splay was one of many relatively minor secondary faults in the vicinity of the Wilzetta fault (see also Sumy *et al.*, 2014). The Nemaha fault (also shown in Fig. 2), strikes nearly north–south through the area of recent seismicity and is part of a major fault system that extends into Kansas. The Nemaha fault has attracted considerable scrutiny in recent years, owing to its length and proximity to Oklahoma City (e.g., Keranen *et al.*, 2014). Figure 1 shows that it is nearly perpendicular to the nearest high-quality S_{Hmax} orientations. Because it dips steeply, Walsh and Zoback (2015b) show that the main trace of the Nemaha fault is essentially impossible to slip in the context of Coulomb faulting theory, and would be considered to present an extremely low seismic hazard. This is consistent with the lack of observed seismicity along the fault, despite the extensive oil and gas development and fluid injection along it.

The overall lack of correlation between the earthquake locations and mapped faults is striking. This seems to reflect two separate but related issues—the earthquakes are principally occurring at 5–6 km depth in crystalline basement (McNamara *et al.* 2015) but the faults are being mapped in the overlaying sedimentary rocks, and the thoroughness of fault mapping is inadequate overall.

Focal Plane Inversions and Faulting Regimes

To determine which of the two possible planes in an earthquake focal plane mechanism is the actual fault plane, we need to know the relative stress magnitudes and stress orientation from independent data. To accomplish this, we subdivided the 316 well-constrained earthquake focal plane mechanisms from St. Louis University and U.S. Geological Survey (Benz and Herrmann, 2014) into seven study areas shown in Figures 1 and 2. In each area, there are a sufficient number of focal plane mechanisms to conduct an inversion to determine the orientation of the three principal stresses as well as the relative value of the intermediate stress defined by the parameter $\Phi(\Phi = (S_2 - S_3)/(S_1 - S_3))$, after Angelier (1990). The focal mechanism inversions utilized the method proposed by Michael (1987) and are discussed in detail by Walsh and Zoback (2016).

The study areas were chosen based on a desire to capture as much of the recent seismicity as possible, and to analyze the focal mechanisms in groups somewhat isolated from each other. In each of the study areas in Oklahoma, there is a minimum of 25 focal mechanisms. In each of the areas in southern Kansas (area 7), there are only 14. With only a limited number of focal plane mechanisms and no wellbore stress orientations for comparison, the result in Kansas is relatively uncertain.

In the six study areas in Oklahoma, we found an excellent correlation between the stress orientations obtained from the wellbore data and the earthquake focal plane mechanisms (see Table 1). The only complexity was observed in area 2, where the focal mechanism inversion in the northern part of the area agrees very well with the orientation of stress from wellbores (and other focal mechanism inversions). In the southern part of area 2, the focal mechanism inversion did not converge on reliable values for the orientation of S_{Hmax} nor Φ.

Table 1 and Figure 2 present both the orientation of stress obtained from both the wellbore data and focal mechanism inversions as well as the style of faulting. In regions 3, 4, 5, and 6, the S_{Hmax} direction is about N84°E. As pointed out by previous workers (see Holland, 2013; McNamara *et al.*, 2015), the style of faulting is strike slip ($S_{Hmax} > S_V > S_{hmin}$). Our inversion results in area 6 are essentially identical to those of Sumy *et al.* (2014), who inverted 110 focal mechanisms associated with the Prague mainshocks and aftershocks. In area 1, the stress direction is similar, but the style of faulting is a combination of strike-slip and normal faulting ($S_{Hmax} \cong S_V > S_{hmin}$). In areas 2N and 7, the style of faulting is dominated by normal faulting ($S_V > S_{Hmax} > S_{hmin}$) and the S_{Hmax} direction is about N80°E. Thus, while there is relatively little change in stress orientation, stress magnitudes are clearly less compressive in northernmost Oklahoma and southern Kansas than in the central part of Oklahoma.

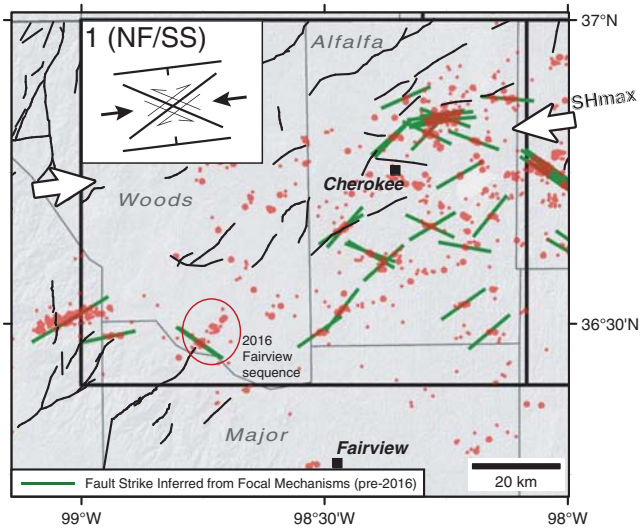

Figure 3. The Fairview earthquake sequence occurred in early 2016 in the southwestern part of study area 1. The location of this sequence is indicated by the red circle and label. Red dots represent local earthquake epicenters, scaled according to moment magnitude. The green lines represent the planes most likely to have slipped during the events for which focal mechanisms are available. Only earthquakes (and likely fault planes) are shown through the end of 2015. Only one focal plane mechanism is available in the area of the Fairview sequence. It indicates slip on a plane striking normal to the earthquakes in the area. The inset to the upper left illustrates the preferred strike-slip and normal fault planes that are predicted by Mohr–Coulomb-faulting theory for an N83°E S_{Hmax} orientation and a stress state in which $S_{\mathrm{Hmax}} \cong S_V > S_{\mathrm{hmin}}$.

Recalling that the style of faulting in the earthquake on the Meers fault was a combination of reverse and strike-slip faulting, there appears to be an overall decrease in compressive stress from strike slip/reverse in the Lawton area to strike slip in central Oklahoma to strike-slip/normal and normal faulting in northern Oklahoma and southern Kansas.

Mapping Faults with Stress and Focal Mechanisms

With independent stress orientations obtained from the wellbore data and the supportive stress orientations and relative stress magnitudes from the inversions of the focal plane mechanisms, we can utilize the Mohr–Coulomb failure criterion to determine which nodal plane is the likely fault plane in any given focal mechanism. Zoback (1992b) and Hurd and Zoback (2012) carried out a similar analysis in the central and eastern United States. We utilized a coefficient of friction of 0.8 in our study, which is consistent with laboratory observations (Byerlee, 1978) and *in situ* observations (e.g., Zoback and Townend, 2001). We evaluated the ratio of shear to normal stress for each of the two nodal planes of the focal plane mechanism and assume the plane with the higher ratio is the likely fault plane. We assume near-hydrostatic pore pressure at the 5–6 km depth of most earthquakes in north-central Oklahoma (McNamara *et al.*, 2015). Pore pressures throughout this region are slightly subhydrostatic (about 4%) in the Arbuckle Formation that lies immediately above the crystalline basement (Nelson *et al.*, 2015). Because the basement is in direct contact with the Arbuckle Formation, it is likely that the same slightly subhydrostatic pressure characterizes the basement rocks at the 5–6 km depth of the earthquakes. The assumed coefficient of friction and slight subhydrostatic pore pressure have no impact on the determination of the likely fault planes. Table A3 lists the focal plane mechanisms and the likely fault planes.

Figures 3 and 4 illustrate how identification of fault planes can be used to supplement knowledge about potentially seismogenic faults and potential earthquake hazard. Figure 3 shows mapped faults and recent seismicity in area 1 through the end of 2015. As shown, there are a number of northeast–southwest-trending faults mapped in the area. As seen in Figure 2, the great majority of earthquakes are not occurring on the mapped faults. Although there are several alignments of epicenters that appear to trend subparallel to the mapped faults, we utilize here the orientations of likely faults inferred from the focal plane mechanisms to augment knowledge of location and orientations of unmapped faults that might be triggered by saltwater injection in the future. Although there is only a single-wellbore stress measurement in study area 1 (and one just to the west), the focal mechanism inversion indicates an S_{Hmax} orientation of about N83°E (the same as the wellbore stress measurements) and a strike-slip/normal-faulting stress field. As illustrated in the Figure 3 inset, near-vertical faults striking about N53°E and N113°E would be oriented appropriately for potentially active strike-slip faults, as would steeply dipping normal faults striking approximately N83°E, subparallel to S_{Hmax}. The green solid lines in Figure 3 show the likely faults associated with the earthquake focal plane mechanisms. Note that a number of these inferred fault

Table 1
Stress Directions from Wells and Focal Mechanisms

Area	Focal Mechanism Inversion S_{Hmax} Azimuth (°)	Φ	S1 Plunge (°)	Number of Focal Mechanisms	Number of Wellbores	Mean Wellbore S_{Hmax} (°)
1	83 ± 3	0.97	14.9	42	1	80
2N	71 ± 6	0.77	86.1	61	7	72
3	82 ± 6	0.82	3.5	117	9	84
4	82 ± 4	0.69	0.6	27	4	77
5	83 ± 2	0.70	1.0	44	2	84
6	84 ± 3	0.62	4.5	25	1	83

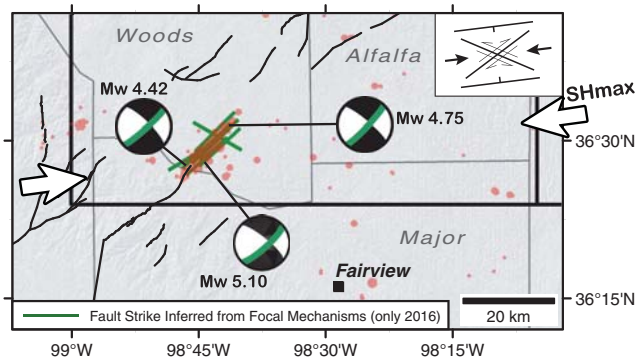

Figure 4. Detail of earthquakes through the end of March 2016 and likely fault planes in the area of the Fairview sequence. Both the locations of the epicenters and orientations of the likely fault planes in the larger earthquakes indicate a northeast extension of the mapped fault to the southwest of the seismicity. The inset to the upper right again reflects optimal fault orientations as in Figure 3.

planes coincide with earthquake epicenters and establish the orientation of the faults associated with these earthquakes. Just north of Cherokee, we see a number of fault planes that suggest both strike-slip faulting on conjugate planes and normal faulting on planes with the orientations noted above. In the area where the 2016 Fairview sequence (named for the town about 40 km to the southeast) will occur, there are two focal plane mechanisms that define likely fault planes that strike to the northwest (there are two green lines that plot right on top of each other). Even though the seismicity and mapped fault trend to the northeast in this area, these earthquakes appear to define a conjugate strike-slip fault that is not associated with the seismicity prior to the Fairview sequence.

The Fairview sequence involved three sizeable earthquakes (and many smaller events) in January 2016. The sequence includes magnitude 5.1, 4.7, and 4.2 events (and many smaller earthquakes) that occurred between 7 and 14 January. The focal plane mechanisms of these events are shown in Figure 4. The orientations of the likely faults and the epicenters of earthquakes that occurred in early 2016 are shown by green lines. As the northeast-trending plane of the focal plane mechanisms is the most likely fault for each of the three largest earthquakes, it suggests an extension of the northeast-trending fault shown on the map. If this fault connects to the fault segments to the northeast with the same overall strike of potentially active faults in this area, it could represent the potential for larger earthquakes to occur in this area.

Conclusions

A remarkably consistent N80–90°E S_{Hmax} orientation characterizes the region of most intense earthquake activity in north-central Oklahoma. Stress magnitudes transition from strike-slip faulting in central Oklahoma to strike-slip and normal faulting in northernmost Oklahoma and southern Kansas. Knowledge of the stress field in this area allows us to identify the likely fault planes in 316 well-constrained earthquake focal plane mechanisms and identify potentially active faults that are currently unmapped and potentially pose a previously unrecognized seismic hazard. In this regard, it is noteworthy that the largest earthquake to have occurred in Oklahoma until recently (the M_w 5.6 event in the 2011 Prague sequence) occurred on a relatively minor splay of the Wilzetta fault that would be expected to be potentially active in the current stress field. The September 2016 M_w 5.8 Pawnee event occurred at the northern edge of area 4 on an unmapped N70°W-trending strike-slip fault expected to be active in the local stress field.

Data and Resources

The well logs provided by Apache Corporation, BP, Chesapeake Energy, Devon Energy, EOG, and Newfield Exploration Company are proprietary. They cannot be released to the public. The maps in Figures 1–4 were made using ArcGIS 10.4 (ESRI 2011. ArcGIS Desktop: Release 10. Redlands, California: Environmental Systems Research Institute). All other data used in this article came from published sources listed in the references.

Acknowledgments

We thank Apache Corporation, BP, Chesapeake Energy, Devon Energy, and Newfield Exploration Company for providing the wellbore stress data we analyzed. F. Rall Walsh contributed to the stress inversions and Jens-Erik Lund Snee provided assistance with preparation of the maps in Figures 1–4. The Stanford Center for Induced and Triggered Seismicity (SCITS) industrial affiliates program provided financial support for this work. This work was also funded in part by 2014–2015 and 2015–2016 awards from the Society of Exploration Geophysicists (SEG) Scholarships program and by a 2013–2014 Graduate Fellowship from the American Meteorological Society (AMS).

References

Angelier, J. (1990). Inversion of field data in fault tectonics to obtain the regional stress: III. A new rapid direct inversion method by analytical means, *Geophys. J. Int.* **103,** 363–376.

Benz, H. M., and R. B. Herrmann (2014). Rapid estimates of the source time function and M_w using empirical Green's function deconvolution, *Bull. Seismol. Soc. Am.* **104,** 1812–1819.

Byerlee, J. (1978). Friction of rocks, *Pure Appl. Geophys.* **116,** 615–626.

Carter, L. S., S. A. Kelley, D. D. Blackwell, and N. D. Naeser (1998). Heat flow and thermal history of the Anadarko Basin, Oklahoma, *AAPG Bulletin* **82,** 291–316.

Crone, A. J., and K. V. Luza (1990). Style and timing of Holocene surface faulting on the Meers fault, southwestern Oklahoma, *Geol. Soc. Am. Bull.* **102,** 1–17.

Darold, A. P., and A. A. Holland (2015). Preliminary Oklahoma fault orientations,*Oklahoma Geol. Surv. Open-File Rept. OF4-2015*.

Heidbach, O., M. Tingay, A. Barth, J. Reinecker, D. Kurfeß, and B. Müller (2010). Global crustal stress pattern based on the World Stress Map database release 2008, *Tectonophysics* **482,** 3–15.

Herrmann, R. (2016). SLU North America Moment Tensor catalog in CSV format with TABS separating b columns, http://www.eas.slu.edu/eqc/eqc_mt/MECH.NA/MECHFIG/mech.html (last accessed July 2016).

Holland, A. A. (2013). Earthquakes triggered by hydraulic fracturing in south-central Oklahoma, *Bull. Seismol. Soc. Am.* **103,** 1784–1792.

Hurd, O., and M. D. Zoback (2012). Regional stress orientations and slip compatibility of earthquake focal planes in the New Madrid seismic zone, *Seismol. Res. Lett.* **83,** 672–679.

Johnson, K. S (1989). Geologic evolution of the Anadarko basin, in *Anadarko Basin Symposium: Oklahoma Geological Survey Circular 90*, K. S. Johnson (Editor), Oklahoma Geological Survey, Norman, Oklahoma, 3–12.

Keranen, K. M., H. M. Savage, G. A. Abers, and E. S. Cochran (2013). Potentially induced earthquakes in Oklahoma, USA: Links between wastewater injection and the 2011 M_w 5.7 earthquake sequence, *Geology* **41,** 699–702.

Keranen, K. M., M. Weingarten, G. A. Abers, B. A. Bekins, and S. Ge (2014). Sharp increase in central Oklahoma seismicity since 2008 induced by massive wastewater injection, *Science* **345,** 448–451.

Lund Snee, J.-E., and M. D. Zoback (2016). State of stress in Texas: Implications for induced seismicity, *Geophys. Res. Lett.* **43,** 10,208–10,214, doi: 10.1002/2016GL070974.

Luza, K. V. (1989). Neotectonics and seismicity of the Anadarko Basin, in *Anadarko Basin Symposium: Oklahoma Geological Survey Circular 90*, K. S. Johnson (Editor), Oklahoma Geological Survey, Norman, Oklahoma, 121–132.

Luza, K. V., R. F. Madole, and A. J. Crone (1987). Investigation of the Meers fault in southwestern Oklahoma, *No. NUREG/CR-4937*, Oklahoma University, Norman, Oklahoma, Nuclear Regulatory Commission, Washington, D.C. , Division of Engineering Research.

McNamara, D. E., H. M. Benz, R. B. Herrmann, E. A. Bergman, P. Earle, A. A. Holland, R. Baldwin, and A. Gassner (2015). Earthquake hypocenters and focal mechanisms in central Oklahoma reveal a complex system of reactivated subsurface strike-slip faulting, *Geophys. Res. Lett.* **42,** 2742–2749.

Michael, A. J. (1987). Use of focal mechanisms to determine stress: a control study, *J. Geophys. Res.* **92,** 357–368.

Nelson, P. H., N. J. Gianoutsos, and R. M. Drake II (2015). Underpressure in Mesozoic and Paleozoic rock units in the Midcontinent of the United States, *AAPG Bulletin* **99,** 1861–1892.

Sumy, D., E. Cochran, K. Keranen, M. Wei, and G. Albers (2014). Observations of static Coulomb stress triggering of the November 2011, M 5.7 Oklahoma earthquake sequence, *J. Geophys. Res.* **119,** no. 3, 1904–1923.

U.S. Geological Survey (2016). Search Earthquake Archives, http://earthquake.usgs.gov/earthquakes/search/ (last accessed September 2016).

Walsh, F. R., and M. D. Zoback (2015a). Oklahoma's recent earthquakes and saltwater disposal, *Sci. Adv.* **1,** e1500195.

Walsh, F. R., and M. D. Zoback (2015b). Quantitative assessment of potentially active faults in Oklahoma utilizing detailed information on in situ stress orientation and relative magnitude, Abstract S22A-05 presented at the *Fall meeting, AGU*, San Francisco, California, 15 December.

Walsh, F. R., and M. D. Zoback (2016). Probabilistic assessment of potential fault slip related to injection induced earthquakes: Application to north-central Oklahoma, USA, *Geology*, Data Repository item 2016334, doi: 10.1130/G38275.1.

Zoback, M. D. (2007). *Reservoir Geomechanics*, Cambridge University Press, Cambridge, United Kingdom, 449 pp.

Zoback, M. D., and J. Townend (2001). Implications of hydrostatic pore pressures and high crustal strength for the deformation of intraplate lithosphere, *Tectonophysics* **336,** 19–30.

Zoback, M. D., and M. L. Zoback (1991). Tectonic stress field of North America and relative plate motions, *Neotectonics of North America* **1,** 339–366.

Zoback, M. L. (1992a). First- and second-order patterns of stress in the lithosphere: The world stress map project, *J. Geophys. Res.* **97,** 11,703–11,728.

Zoback, M. L. (1992b). Stress field constraints on intraplate seismicity in eastern North America, *J. Geophys. Res.* **97,** 11,761–11,782.

Appendix

The tables below provide the detailed quality ranking system used in this data compilation (Table A1) and a complete list of every new data point shown in the figures (Table A2). Table A3 is a list of the focal plane mechanisms in the analysis area and the orientation of the nodal plane most consistent with the stress field in that area.

Table A1

Quality Ranking System for Wellbore S_{Hmax} Orientations (Modified after Zoback and Zoback, 1991; Zoback, 1992a)

Stress Indicator	A	B	C	D (Excluded from Map)
Drilling-induced tensile fractures (DITF)	Ten or more distinct tensile fractures in a single well with std. dev. ≤ 12° and encompassing a vertical depth of 300 m, or more	At least six distinct tensile fractures in a single well with std. dev. ≤ 20° and encompassing a combined length > 100 m	At least four distinct tensile fractures with std. dev. ≤ 25° if numerical std. dev. is available and encompassing a combined length > 30 m	Less than four consistently oriented tensile fractures with < 30 m combined length in a single well. Tensile fracture orientations in a single well with std. dev. ≥ 25° if numerical std. dev. is available
Shear-velocity anisotropy	≥2% anisotropy present at a consistent wellbore azimuth, with highest and lowest observations at least 300 m apart, std. dev. of fast azimuth ≤ 12°	≥2% anisotropy present at a consistent wellbore azimuth, with highest and lowest observations at least 100 m apart, std. dev. of fast azimuth ≤ 20°	≥2% anisotropy present at a consistent wellbore azimuth, with highest and lowest observations at least 30 m apart, std. dev. of fast azimuth ≤ 25° if numerical std. dev. is available	Maximum anisotropy < 2%, highest and lowest observations < 30 m, std. dev. of fast azimuth > 25°
Wellbore breakout	Ten or more distinct breakout zones in a single well with std. dev. ≤ 12° and/or combined length > 300 m. Average of breakouts in two or more wells in close geographic proximity with combined length > 300 m and std. dev. ≤ 12°	At least six distinct breakout zones in a single well with std. dev. ≤ 20° and/or combined length > 100 m	At least four distinct breakouts with std. dev. ≤ 25° if numerical std. dev. is available and/or combined length > 30 m	Less than four consistently oriented breakout or > 30 m combined length in a single well. Breakouts in a single well with std. dev. ≥ 25° if numerical std. dev. is available

Table A2

Wellbore S_{Hmax} Orientations by Latitude, Longitude, and Quality Ranking

Latitude (°)	Longitude (°)	S_{Hmax} Azimuth (°)	Quality Ranking	Data Source
34.73	−96.19	85	B	DITF
36.07	−97.52	86	B	DITF
36.03	−97.02	76	A	DITF
36.08	−97.42	83	B	DITF
36.07	−97.00	73	A	DITF
36.10	−97.34	81	C	DITF
36.20	−97.59	79	C	DITF
36.12	−97.41	86	A	DITF
36.06	−97.33	82	B	DITF
36.85	−96.87	91	B	DITF
35.57	−96.94	80	A	DITF
36.34	−97.01	81	C	DITF
36.77	−97.71	79	B	DITF
36.83	−97.77	79	A	DITF
36.28	−97.58	85	C	DITF
36.97	−97.66	73	A	DITF
35.79	−97.39	86	B	DITF
36.82	−97.61	70	C	DITF
36.74	−97.77	70	B	DITF
36.83	−97.66	68	A	DITF
36.66	−97.64	59	A	DITF
36.46	−97.28	82	A	DITF
36.20	−97.04	79	C	DITF
36.91	−97.68	69	A	DITF
34.39	−95.98	76	A	DITF
35.67	−97.68	80	C	DITF
34.29	−97.15	72	B	DITF
34.07	−95.92	75	B	DITF
34.68	−98.20	56	A	DITF
35.91	−99.28	83	A	DITF
36.13	−99.86	90	B	DITF
34.80	−97.84	65	B	DITF
34.25	−96.91	89	C	DITF
34.23	−96.89	83	B	DITF
33.95	−97.00	53	C	DITF
34.10	−96.74	72	B	DITF
34.10	−96.68	60	B	DITF
35.63	−99.77	80	B	DITF
34.57	−98.00	65	A	DITF
34.56	−98.06	63	C	DITF
34.40	−98.00	82	B	DITF
34.48	−98.07	81	B	DITF
35.16	−98.90	70	B	DITF
36.82	−99.12	75	C	DITF
36.90	−98.68	80	C	DITF
35.96	−98.18	90	A	DITF
34.65	−96.36	100	B	DITF
35.68	−97.92	85	B	DITF
34.49	−96.17	88	B	DITF
34.68	−96.20	88	C	DITF
35.78	−99.50	63	C	DITF
35.41	−99.17	90	C	DITF
35.41	−99.99	85	C	DITF
35.42	−99.97	75	C	DITF
36.01	−100.17	88	B	DITF
36.23	−97.78	89	A	DITF
36.16	−100.11	96	A	DITF
35.14	−98.36	71	A	DITF
34.95	−97.99	65	A	DITF
34.96	−96.43	88	C	DITF
35.04	−97.15	85	B	DITF
35.65	−97.13	88	B	DITF
34.35	−96.24	75	A	DITF
35.93	−98.75	81	C	SVA*
35.91	−98.78	81	C	SVA
35.49	−98.48	86	C	SVA
35.57	−98.13	74	C	SVA
35.67	−98.30	86	C	SVA
35.80	−99.25	85	C	SVA
35.63	−99.21	95	C	SVA
34.79	−96.26	90	C	SVA
34.65	−96.10	90	B	SVA
34.40	−96.18	69	B	SVA
−95.19	34.68	72	C	SVA
−99.76	35.72	100	C	SVA

*SVA, shear-velocity anisotropy.

Table A3
Focal Mechanisms (after Herrmann, 2016) by Area and Strike and Dip of Preferred Slip Plane

Area	Latitude (°)	Longitude (°)	Magnitude (M_w)	Date (yyyy/mm/dd) and Time (hh:mm) of Earthquake	Strike (°)	Dip (°)
1	36.82	−98.23	3.32	2014/04/07 03:25	263	56
1	36.59	−98.32	3.39	2014/05/30 21:42	48	80
1	36.64	−98.24	3.32	2014/07/25 04:56	239	75
1	36.83	−98.25	3.47	2014/08/18 01:25	290	65
1	36.52	−98.98	3.37	2014/10/31 06:23	240	60
1	36.87	−98.33	3.67	2014/11/24 19:05	246	52
1	36.87	−98.16	3.84	2014/12/14 09:14	275	65
1	36.77	−98.18	3.66	2015/01/19 10:19	290	85
1	36.8	−98.34	3.39	2015/01/24 15:36	44	76
1	36.81	−98.37	3.65	2015/01/30 14:24	48	71
1	36.52	−98.18	3.4	2015/02/05 07:06	55	76
1	36.79	−98.27	4.12	2015/02/05 15:08	295	80
1	36.47	−98.18	3.18	2015/04/03 02:16	230	90
1	36.54	−98.98	3.71	2015/05/01 07:32	238	81
1	36.59	−98.36	3.44	2015/05/22 10:57	290	85
1	36.72	−98.19	3.4	2015/06/27 03:31	60	70
1	36.66	−98.15	3.38	2015/06/28 01:35	219	72
1	36.65	−98.23	3.8	2015/07/10 23:09	115	80
1	36.5	−98.44	3.52	2015/07/17 12:30	218	80
1	36.85	−98.2	3.59	2015/07/20 20:54	265	50
1	36.82	−98.25	3.12	2015/07/21 11:16	265	55
1	36.61	−98.4	3.45	2015/07/24 12:31	120	80
1	36.8	−98.23	3.43	2015/08/20 00:47	260	50
1	36.48	−98.5	3.5	2015/09/02 13:50	55	90
1	36.5	−98.93	3.62	2015/09/16 04:48	258	45
1	36.61	−98.15	3.48	2015/10/02 05:58	280	80
1	36.45	−98.73	4.29	2015/11/15 09:45	305	80
1	36.66	−98.46	4.64	2015/11/19 07:42	221	80
1	36.63	−98.45	3.3	2015/11/19 12:03	56	75
1	36.83	−98.29	4.29	2015/11/23 21:17	255	50
1	36.82	−98.29	3.25	2015/11/24 00:54	224	60
1	36.83	−98.26	3.18	2015/12/04 05:08	80	65
1	36.45	−98.69	3.94	2015/12/06 01:01	305	75
1	36.48	−98.73	4.42	2016/01/07 04:27	48	81
1	36.49	−98.71	4.75	2016/01/07 04:27	43	80
1	36.47	−98.67	3.59	2016/01/07 08:37	47	80
1	36.48	−98.7	3.59	2016/01/07 19:59	45	85
1	36.5	−98.67	3.81	2016/01/08 13:36	225	90
1	36.46	−98.67	3.44	2016/01/11 02:01	59	70
1	36.49	−98.68	3.77	2016/01/19 20:45	300	75
1	36.4905	−98.741	5.1	2016/02/13 17:07	47	72
2	36.57	−97.62	3.49	2014/05/08 20:40	100	70
2	36.56	−97.59	3.85	2014/05/09 18:52	90	80
2	36.68	−97.82	3.93	2014/06/20 23:10	71	57
2	36.83	−97.85	3.36	2014/06/23 13:44	295	85
2	36.83	−97.7	3.23	2014/06/26 14:02	315	90
2	36.72	−97.81	3.73	2014/06/27 22:35	110	60
2	36.7	−97.86	3.94	2014/07/14 07:15	100	60
2	36.73	−97.99	4.26	2014/07/29 02:46	305	65
2	36.74	−98.02	3.08	2014/08/01 14:19	300	60
2	36.73	−98.03	3.15	2014/08/01 14:44	125	80
2	36.84	−97.84	3.47	2014/08/17 06:18	295	90
2	36.84	−97.83	3.26	2014/08/17 06:31	295	90
2	36.83	−97.85	3.29	2014/08/17 15:59	300	80
2	36.59	−97.99	3.36	2014/08/31 07:20	120	70
2	36.62	−97.69	3.46	2014/09/06 18:53	236	85
2	36.81	−97.72	3.7	2014/09/08 16:21	60	45
2	36.61	−97.95	3.43	2014/09/14 12:01	125	75
2	36.58	−97.6	3.71	2014/09/19 01:31	71	61
2	36.79	−97.72	3.66	2014/11/25 14:43	110	85

(*continued*)

Table A3 (*Continued*)

Area	Latitude (°)	Longitude (°)	Magnitude (M_w)	Date (yyyy/mm/dd) and Time (hh:mm) of Earthquake	Strike (°)	Dip (°)
2	36.58	−97.61	3.93	2014/11/30 10:24	75	85
2	36.75	−98.04	3.63	2014/12/11 07:53	305	65
2	36.92	−97.63	3.36	2015/01/20 15:27	65	90
2	36.94	−97.6	3.62	2015/01/25 09:36	60	80
2	36.63	−97.7	3.89	2015/01/27 15:58	71	61
2	36.95	−97.62	3.67	2015/02/01 18:06	60	85
2	36.95	−97.62	3.42	2015/02/13 17:42	288	50
2	36.59	−97.63	3.66	2015/03/07 21:11	260	80
2	36.6	−97.67	3.14	2015/03/07 22:46	258	86
2	36.74	−97.52	3.33	2015/03/10 04:21	110	85
2	36.61	−97.67	3.86	2015/03/12 20:34	245	90
2	36.59	−97.61	3.79	2015/03/17 23:45	85	85
2	36.62	−97.64	3.84	2015/03/23 23:29	71	75
2	36.58	−97.62	3.36	2015/03/25 00:15	80	80
2	36.62	−97.65	3.82	2015/04/06 15:30	65	85
2	36.91	−97.64	3.34	2015/04/18 18:34	52	80
2	36.82	−97.86	3.37	2015/04/20 12:08	61	85
2	36.61	−97.65	3.63	2015/04/23 06:20	312	61
2	36.99	−97.94	3.59	2015/04/28 22:18	70	68
2	36.83	−97.69	3.21	2015/05/23 10:46	231	85
2	36.93	−97.62	3.43	2015/06/02 07:55	76	42
2	36.67	−97.84	3.31	2015/08/01 20:28	275	65
2	36.83	−97.8	3.99	2015/08/14 21:25	120	85
2	36.82	−97.78	3.8	2015/08/22 08:46	125	75
2	36.88	−97.64	3.38	2015/09/10 19:26	100	55
2	36.71	−97.91	4.33	2015/10/10 09:20	95	50
2	36.69	−97.93	3.39	2015/10/10 15:20	95	45
2	36.71	−97.82	3.12	2015/10/19 04:55	50	90
2	36.92	−97.84	4.18	2015/11/07 11:11	90	65
2	36.93	−97.82	3.75	2015/11/07 18:29	100	60
2	36.93	−97.81	3.5	2015/11/11 01:39	100	65
2	36.93	−97.82	3.97	2015/11/20 22:40	85	60
2	36.91	−97.82	3.46	2015/11/20 22:55	90	60
2	36.91	−97.8	3.11	2015/11/26 00:56	260	75
2	36.75	−98.02	4.67	2015/11/30 09:49	305	80
2	36.92	−97.81	3.27	2015/11/30 21:28	265	70
2	36.93	−97.8	3.63	2015/12/08 00:08	80	60
2	36.73	−97.97	3.46	2015/12/25 19:12	130	70
2	36.93	−97.8	3.47	2016/01/14 23:15	85	60
2	36.91	−97.64	3.47	2016/01/24 10:01	112	41
2	36.9	−97.98	3.21	2016/01/26 06:24	305	85
2	36.81	−97.77	3.36	2016/02/06 20:39	48	85
3	35.9	−97.31	3.65	2016/12/29 08:14	300	85
3	35.88	−97.26	4.07	2014/02/09 02:16	305	80
3	35.78	−97.47	3.71	2014/02/17 04:54	300	70
3	36.04	−97.33	3.45	2014/02/23 09:15	220	90
3	35.9	−97.27	3.59	2014/03/11 12:55	220	71
3	35.83	−97.25	3.81	2014/03/22 03:05	115	85
3	36.14	−97.59	4.23	2014/03/30 06:51	44	85
3	36.14	−97.62	3.26	2014/03/30 08:07	227	66
3	36.13	−97.64	3.31	2014/03/30 08:10	226	61
3	36.14	−97.62	3.87	2014/03/30 08:42	40	80
3	36.13	−97.65	4.04	2014/03/30 14:09	44	70
3	35.89	−97.28	3.11	2014/04/04 18:54	245	85
3	36.13	−97.63	3.77	2014/04/05 12:42	40	85
3	35.92	−97.26	3.7	2014/04/06 14:58	230	80
3	35.88	−97.19	4.16	2014/04/07 16:03	240	85
3	35.79	−97.47	4	2014/04/10 07:33	39	67
3	35.78	−97.47	3.48	2014/04/10 08:19	305	90
3	36.26	−97.24	3.77	2014/04/12 05:32	227	74
3	36.27	−97.25	3.77	2014/04/19 10:43	224	76
3	35.79	−97.48	3.37	2014/05/15 20:23	300	80

(*continued*)

Table A3 (*Continued*)

Area	Latitude (°)	Longitude (°)	Magnitude (M_w)	Date (yyyy/mm/dd) and Time (hh:mm) of Earthquake	Strike (°)	Dip (°)
3	35.79	−97.48	3.63	2014/05/22 02:46	105	75
3	35.98	−97.18	3.24	2014/06/18 14:08	95	65
3	35.99	−97.18	3.34	2014/06/20 14:46	95	45
3	35.8	−97.48	3.54	2014/06/26 05:26	290	65
3	35.79	−97.49	3.49	2014/06/26 05:38	300	75
3	35.79	−97.51	3.25	2014/06/26 06:13	285	85
3	35.89	−97.26	3.61	2014/06/26 23:28	110	80
3	35.91	−97.3	3.65	2014/06/27 15:09	95	75
3	35.87	−97.27	4.05	2014/07/12 17:11	220	80
3	35.87	−97.31	3.26	2014/07/14 16:50	233	80
3	35.9	−97.31	3.27	2014/07/23 02:02	100	85
3	35.88	−97.31	2.92	2014/07/23 14:03	105	90
3	35.83	−97.42	3.36	2014/08/04 15:30	300	90
3	35.82	−97.41	3.34	2014/08/08 20:21	305	85
3	35.82	−97.47	4.32	2014/08/19 12:41	300	70
3	35.84	−97.43	3.03	2014/08/23 11:06	115	85
3	35.84	−97.47	3.07	2014/08/26 16:05	290	70
3	36.2	−97.42	3.25	2014/09/04 23:32	300	85
3	36.2	−97.42	3.37	2014/09/09 09:06	305	85
3	36.17	−97.27	3.67	2014/09/12 14:41	295	70
3	35.82	−97.43	3.86	2014/09/15 20:08	300	75
3	36.18	−97.25	3.34	2014/09/17 13:21	295	65
3	36.2	−97.27	3.67	2014/09/18 07:12	300	90
3	35.82	−97.42	3.55	2014/09/19 17:23	40	76
3	35.84	−97.44	3.36	2014/09/27 12:14	44	72
3	36.23	−97.56	3.96	2014/09/30 03:01	120	80
3	36.21	−97.55	3.2	2014/09/30 06:06	295	80
3	36.17	−97.28	3.28	2014/10/08 19:44	285	60
3	36.05	−97.26	3.31	2014/10/30 18:57	235	85
3	36.06	−97.25	2.99	2014/11/01 06:03	240	80
3	36.33	−97.53	3.69	2014/11/24 06:36	65	90
3	35.84	−97.43	3.34	2014/11/25 22:04	280	60
3	35.82	−97.45	3.6	2014/12/07 22:13	47	80
3	36.16	−97.47	3.41	2014/12/18 23:06	250	85
3	35.83	−97.42	3.52	2014/12/25 20:32	48	66
3	35.84	−97.44	3.59	2015/01/04 21:37	285	50
3	36.26	−97.26	3.61	2015/01/05 22:06	290	90
3	36.26	−97.28	3.71	2015/01/05 22:27	105	85
3	35.82	−97.43	3.71	2015/01/07 19:41	285	60
3	35.83	−97.43	3.53	2015/01/09 06:44	57	62
3	35.82	−97.42	3.37	2015/01/11 10:28	105	80
3	36.26	−97.27	4.24	2015/01/27 11:31	105	90
3	36.27	−97.28	3.8	2015/02/07 18:40	110	80
3	35.87	−97.34	3.5	2015/02/16 09:50	120	55
3	35.83	−97.44	3.69	2015/03/09 03:24	229	67
3	35.85	−97.44	3.14	2015/03/09 10:48	53	56
3	36.27	−97.29	3.28	2015/03/21 19:58	100	90
3	36.13	−97.58	3.42	2015/03/23 20:16	242	52
3	36.34	−97.17	3.58	2015/03/24 00:27	120	90
3	36.15	−97.54	3.64	2015/04/04 00:49	100	45
3	36.13	−97.57	3.3	2015/04/04 05:02	115	45
3	36.33	−97.52	3.35	2015/04/04 08:35	255	85
3	36.13	−97.57	4.01	2015/04/04 13:21	72	42
3	36.33	−97.52	3.45	2015/04/07 17:25	80	90
3	35.85	−97.42	4.07	2015/04/08 20:51	295	75
3	35.94	−97.33	3.49	2015/04/17 08:37	110	80
3	35.94	−97.34	3.67	2015/04/17 09:08	295	90
3	35.94	−97.34	4.09	2015/04/19 05:27	115	90
3	35.94	−97.34	3.45	2015/04/19 06:28	95	40
3	36.28	−97.52	3.45	2015/04/26 19:07	285	80
3	35.94	−97.36	4.07	2015/04/27 22:22	115	85
3	36.29	−97.53	3.75	2015/04/29 16:42	45	71

(*continued*)

Table A3 (*Continued*)

Area	Latitude (°)	Longitude (°)	Magnitude (M_w)	Date (yyyy/mm/dd) and Time (hh:mm) of Earthquake	Strike (°)	Dip (°)
3	35.83	−97.46	3.41	2015/05/18 02:52	229	72
3	36.16	−97.3	3.44	2015/05/28 12:00	285	85
3	36.28	−97.54	3.84	2015/06/08 21:36	125	75
3	36.29	−97.52	3.65	2015/06/09 01:26	42	71
3	36.3	−97.53	3.37	2015/06/10 13:05	233	61
3	36.28	−97.55	3.45	2015/06/11 23:28	290	90
3	36.29	−97.51	3.65	2015/06/11 23:31	295	85
3	36.29	−97.54	3.59	2015/06/12 04:38	120	65
3	36.27	−97.39	3.29	2015/06/13 20:54	305	85
3	36.29	−97.52	3.84	2015/06/14 18:17	47	80
3	36.29	−97.53	3.34	2015/06/14 19:10	67	52
3	36.29	−97.52	4.17	2015/06/17 19:17	60	54
3	36.22	−97.56	3.41	2015/06/22 04:54	290	90
3	36.28	−97.51	3.44	2015/07/03 05:19	44	63
3	36.28	−97.51	3.14	2015/07/04 11:57	231	80
3	36	−97.57	3.42	2015/07/15 08:57	120	80
3	36.29	−97.61	3.21	2015/07/21 08:46	238	57
3	36	−97.57	3.62	2015/07/25 11:14	280	75
3	36.01	−97.57	3.6	2015/07/26 09:54	280	65
3	36	−97.57	3.84	2015/07/27 17:49	95	90
3	36.01	−97.58	4.47	2015/07/27 18:12	100	80
3	36	−97.58	4.13	2015/07/28 01:18	275	80
3	36.28	−97.53	3.2	2015/08/05 14:23	235	80
3	36.28	−97.52	3.11	2015/08/13 04:15	230	75
3	36.09	−97.24	3.3	2015/08/13 20:02	45	85
3	36.29	−97.53	3.31	2015/08/20 08:28	45	85
3	36.05	−97.15	3.2	2015/08/23 16:21	240	90
3	36.05	−97.14	3.23	2015/08/25 12:59	58	80
3	36.19	−97.48	3.36	2015/09/09 03:42	120	75
3	36.26	−97.24	3.65	2015/10/01 05:56	110	85
3	36.32	−97.55	3.39	2015/10/11 10:27	65	90
3	36.09	−97.58	3.47	2015/10/30 20:20	55	85
3	35.94	−97.35	3.92	2015/11/02 16:57	251	85
3	36.13	−97.64	3.32	2015/11/18 12:08	295	70
3	36.09	−97.58	3.54	2015/11/19 14:24	51	80
4	35.82	−96.82	3.3	2010/12/19 05:05	280	45
4	35.94	−96.91	3.54	2014/02/01 09:08	120	85
4	35.83	−96.92	3.63	2014/02/10 23:37	120	90
4	35.97	−96.93	3.45	2014/03/19 20:15	295	85
4	35.82	−96.94	3.26	2014/05/01 10:04	110	80
4	36.39	−96.78	3.47	2014/09/24 05:49	95	60
4	35.95	−96.78	3.91	2014/10/07 16:51	100	90
4	35.96	−96.77	4.16	2014/10/10 13:51	280	90
4	35.78	−97.09	3.2	2014/10/10 16:18	285	80
4	36.03	−97.09	3.81	2014/11/09 20:10	39	78
4	36.04	−97.09	3.67	2014/12/05 03:54	300	85
4	36.36	−96.78	3.87	2014/12/14 21:18	55	71
4	36.36	−97.1	3.59	2015/03/21 10:08	120	80
4	35.85	−97.04	3.63	2015/03/23 17:17	65	90
4	36.31	−96.69	3.54	2015/06/12 22:42	236	85
4	36.11	−97.11	3.43	2015/07/01 17:15	300	70
4	36.29	−96.88	3.35	2015/07/04 01:05	65	90
4	36.04	−97.11	3.57	2015/07/11 09:23	295	85
4	35.97	−96.8	3.27	2015/09/02 14:01	60	85
4	36	−96.8	3.66	2015/09/16 02:30	245	90
4	36.34	−96.79	3.19	2015/09/16 12:09	242	80
4	36	−96.81	3.21	2015/09/18 09:16	240	90
4	36.01	−96.84	3.99	2015/09/18 12:35	240	90
4	35.99	−96.84	3.87	2015/09/25 01:16	55	85
4	36	−96.78	3.09	2015/09/25 01:59	245	90
4	36.01	−96.82	4.21	2015/10/10 22:03	60	90
4	36	−96.82	3.34	2015/11/10 13:36	240	90

(*continued*)

Table A3 (*Continued*)

Area	Latitude (°)	Longitude (°)	Magnitude (M_w)	Date (yyyy/mm/dd) and Time (hh:mm) of Earthquake	Strike (°)	Dip (°)
5	35.59	−97.26	3.81	2010/01/15 15:18	55	65
5	35.57	−97.28	3.67	2010/01/15 15:27	42	60
5	35.57	−97.28	3.61	2010/01/24 07:14	115	85
5	35.53	−97.3	3.17	2010/02/13 05:30	57	80
5	35.56	−97.3	3.01	2010/02/15 03:32	228	71
5	35.63	−97.22	3.38	2010/09/16 21:41	285	85
5	35.59	−97.21	3.47	2010/09/19 22:01	285	70
5	35.2	−97.31	4.33	2010/10/13 14:06	120	80
5	35.63	−97.25	3.93	2010/11/24 22:48	280	90
5	35.61	−97.39	3.52	2013/11/02 09:36	285	65
5	35.59	−97.39	3.41	2013/11/02 14:19	290	60
5	35.59	−97.35	3.65	2013/11/05 04:01	295	90
5	35.63	−97.34	4.48	2013/12/07 18:10	110	70
5	35.64	−97.38	3.35	2014/03/05 14:17	100	60
5	35.74	−97.56	3	2014/03/25 14:01	41	85
5	35.5	−97.22	3.42	2014/03/30 03:08	235	85
5	35.77	−97.5	3.67	2014/04/20 19:07	105	70
5	35.59	−97.4	3.23	2014/05/02 19:44	105	80
5	35.53	−97.22	3.37	2014/05/20 07:30	252	69
5	35.49	−97.25	3.73	2014/05/31 10:18	241	85
5	35.5	−97.24	3.48	2014/06/01 19:54	245	90
5	35.59	−97.41	3.47	2014/06/16 10:31	110	75
5	35.58	−97.33	4.28	2014/06/16 10:47	105	65
5	35.61	−97.37	4.04	2014/06/18 10:53	110	65
5	35.53	−97.14	3.69	2014/07/15 07:19	110	85
5	35.73	−97.4	3.31	2014/07/30 16:21	240	65
5	35.61	−97.39	3.21	2014/08/04 18:23	95	70
5	35.76	−97.5	3.22	2014/10/13 12:24	125	70
5	35.73	−97.53	3.13	2014/10/29 16:53	250	90
5	35.69	−97.38	3.32	2014/11/30 12:18	110	80
5	35.7	−97.37	3.41	2014/12/02 12:04	110	80
5	35.65	−97.26	3.29	2015/03/08 16:48	62	75
5	35.77	−97.42	3.97	2015/06/20 05:10	44	63
5	35.76	−97.41	3.31	2015/06/20 10:56	295	75
5	35.76	−97.38	3.42	2015/06/20 11:21	285	65
5	35.75	−97.38	3.23	2015/06/22 04:00	285	90
5	35.76	−97.4	3.36	2015/06/22 21:06	40	75
5	35.77	−97.41	3.83	2015/06/22 22:16	285	70
5	35.75	−97.39	3.36	2015/06/26 04:35	231	76
5	35.75	−97.39	3.61	2015/06/26 05:54	229	76
5	35.69	−97.39	3.44	2015/08/30 12:19	280	70
5	35.68	−97.4	4.26	2015/12/29 11:39	125	85
5	35.69	−97.43	4.25	2016/01/01 11:39	120	85
5	35.76	−97.37	3.28	2016/01/02 20:26	300	85
6	35.54	−96.75	4.15	2010/02/27 22:22	306	70
6	35.54	−96.74	3.66	2010/03/22 02:37	58	86
6	35.39	−97	3.2	2010/12/12 01:07	46	85
6	35.43	−96.53	3.21	2011/03/31 05:41	300	85
6	35.57	−96.7	4.7	2011/11/05 07:12	300	80
6	35.54	−96.75	5.59	2011/11/06 03:53	235	85
6	35.56	−96.87	3.69	2011/11/06 06:31	234	86
6	35.51	−96.86	3.65	2011/11/06 09:39	50	80
6	35.57	−96.8	3.55	2011/11/06 10:52	232	80
6	35.53	−96.91	3.74	2011/11/06 15:07	51	75
6	35.55	−96.82	3.43	2011/11/06 17:52	54	85
6	35.52	−96.79	3.2	2011/11/07 01:17	246	80
6	35.51	−96.8	3.24	2011/11/07 01:26	230	75
6	35.54	−96.75	4.83	2011/11/08 02:46	95	90
6	35.54	−96.8	3.47	2011/11/08 19:05	40	65
6	35.53	−96.74	3.44	2011/11/24 21:11	225	65
6	35.56	−96.76	3.72	2012/04/16 08:12	120	90
6	35.44	−96.53	3.52	2013/01/04 01:59	300	60

(*continued*)

Table A3 (*Continued*)

Area	Latitude (°)	Longitude (°)	Magnitude (M_w)	Date (yyyy/mm/dd) and Time (hh:mm) of Earthquake	Strike (°)	Dip (°)
6	35.69	−97.09	4.46	2013/04/16 06:56	50	65
6	35.68	−97.1	4.24	2013/04/16 10:16	58	75
6	35.56	−97.12	3.81	2014/07/15 09:08	98	50
6	35.37	−96.49	3.53	2014/08/18 02:50	155	65
6	35.76	−97.09	3.2	2014/10/08 01:48	110	85
6	35.34	−96.53	3.59	2014/11/13 01:28	290	80
6	35.53	−96.76	3.51	2014/11/30 06:59	225	90
7	37.12	−97.78	3.7	2013/12/16 15:09	192	61
7	37.13	−97.77	3.57	2014/02/03 09:03	195	50
7	37.07	−97.79	3.03	2014/07/09 02:10	205	85
7	37.12	−97.79	3.17	2014/07/17 10:40	248	50
7	37.27	−97.6	3.39	2014/09/08 12:56	99	63
7	37.24	−97.97	3.63	2014/09/30 14:55	255	45
7	37.24	−97.9	4.31	2014/10/02 18:01	245	45
7	37.27	−97.62	4.78	2014/11/12 21:40	295	80
7	37.19	−97.89	3.57	2015/01/19 09:54	300	80
7	37.19	−97.89	3.36	2015/01/29 20:21	300	90
7	37.2	−97.9	3.42	2015/02/04 13:20	295	60
7	37.18	−97.91	3.55	2015/02/15 18:27	271	85
7	37.03	−97.91	3.55	2015/05/30 11:21	290	50
7	37.21	−98.01	3.96	2015/06/05 23:12	235	41
7	37.03	−97.93	3.43	2015/10/17 12:12	260	40
7	37.05	−97.94	3.4	2015/10/17 13:20	280	35
7	37.15	−97.61	3.4	2015/10/30 04:37	90	70
7	37.09	−97.62	3.5	2015/11/09 22:42	115	75

Department of Geophysics
Stanford University
397 Panama Mall
Stanford, California 94305
rcalt@stanford.edu
zoback@stanford.edu

Manuscript received 20 May 2016;
Published Online 6 December 2016